

Creating Non-Maxwellian Velocity Distributions in Ultracold Plasmas

J. Castro*, G. Bannasch[†], P. McQuillen*, T. Pohl[†] and T. C. Killian*

**Department of Physics and Astronomy and Rice Quantum Institute, Rice University, Houston, Texas 77005, USA*

[†]Max Planck Institute for the Physics of Complex Systems, 01187 Dresden, Germany

Abstract. We present techniques to perturb, measure and model the ion velocity distribution in an ultracold neutral plasma produced by photoionization of strontium atoms. By optical pumping with circularly polarized light we promote ions with certain velocities to a different spin ground state, and probe the resulting perturbed velocity distribution through laser-induced fluorescence spectroscopy. We discuss various approaches to extract the velocity distribution from our measured spectra, and assess their quality through comparisons with molecular dynamic simulations.

Keywords: Ultracold plasmas, strongly coupled plasmas, fluorescence imaging, optical pumping

PACS: 52.27.Gr, 32.80.Xx, 52.65.Yy

INTRODUCTION

The ability to modify and probe the velocity distribution of particles in plasmas is valuable for studying collective modes [1], transport [2], and thermalization rates in plasmas [3]. Here, we describe the combined application of optical pumping and laser-induced fluorescence (LIF) Doppler spectroscopy to create and characterize perturbed ion velocity distributions in ultracold plasmas. Optical pumping [4] between different hyperfine states provides a powerful method for tagging certain particles in equilibrium systems. Exploiting the Doppler effect, the spin-state modification can be done in a velocity-dependent manner to modify the velocity distribution of a given spin state. On the other hand, LIF spectroscopy is a well established tool for measuring velocity distributions [5] and has been used to probe pure ion plasmas [1] or plasmas created with short pulse lasers [6].

Ultracold plasmas (UCPs), produced by photo-ionization of laser-cooled atoms [7] or cold molecular beams [8] provide a well controlled laboratory to study various plasma physics phenomena, such as collective waves [9, 10, 11, 12, 13, 14, 15], plasma expansion into vacuum [16, 17, 18, 19, 20, 21, 22, 23], correlation effects [24, 25, 26, 27, 28, 29, 30, 31, 32], recombination to form neutral atoms [33, 34, 35, 36, 37, 38], and plasma instabilities [39, 40]. Due to their very low temperatures UCPs also realize an interesting parameter regime [41, 42, 43] in which the ionic plasma component can be strongly coupled. Consequently, the present work opens up new studies of non-equilibrium plasma dynamics in the strong coupling regime.

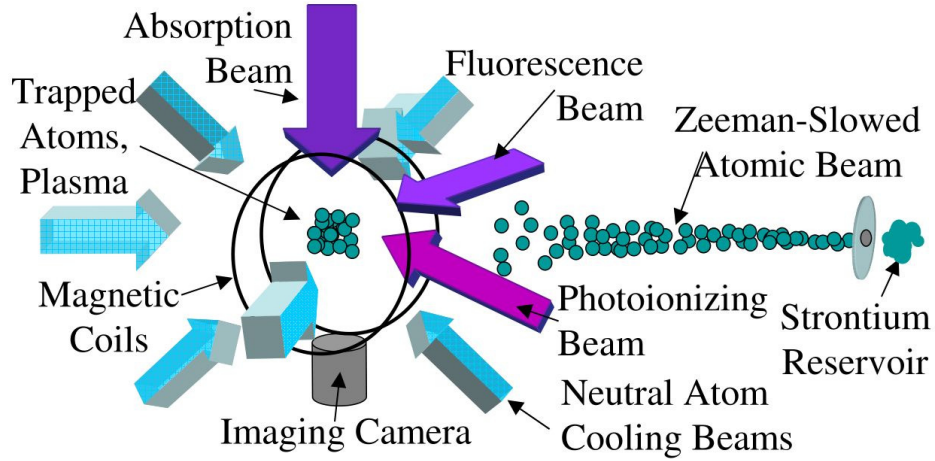


FIGURE 1. Schematics of the experimental setup. Neutral strontium atoms from a heated reservoir are Zeeman-slowed before entering the trapping region. The magneto-optical trap consists of a pair of anti-Helmholtz magnetic coils and six laser beams. 1P_1 trapped atoms are then ionized by the photoionizing laser. The fluorescence probe beam propagates in a direction that is perpendicular to the imaging axis and CCD camera. The complementary absorption probe beam passes through the plasma and falls on the camera. Adapted from [28].

CREATION OF ULTRACOLD NEUTRAL PLASMAS

We create an ultracold neutral plasma through photoionization of laser-cooled strontium atoms in a magneto-optical trap (MOT) [28, 44, 45]. Figure 1 shows our experimental setup. The MOT operates on the dipole-allowed $^1S_0 - ^1P_1$ transition of ^{88}Sr at 461 nm, with transition linewidth, $\gamma/(2\pi) = 30.5$ MHz [46]. The laser-cooled atom cloud is characterized by a temperature of ~ 10 mK and has a spherically symmetric Gaussian density distribution, $n(r) = n_0 \exp(-r^2/2\sigma^2)$, with $\sigma \approx 0.6$ mm and $n_0 \approx 6 \times 10^{10} \text{ cm}^{-3}$. The number of trapped atoms is typically 2×10^8 .

The atoms are ionized via two-photon ionization by two temporally and spatially overlapping, retro-reflected ~ 10 ns laser pulses: the first is obtained from a pulse-amplified laser beam tuned to the cooling transition of the atoms ($^1S_0 - ^1P_1$) at 461 nm and the second one derives from a pulsed dye laser tuned just above the ionization continuum at ~ 412 nm (Figure 2 A).

In this way we ionize ~ 30 -70% of the atoms. The plasma inherits its density distribution from the neutral atoms, resulting in peak electron and ion densities as high as $n_{0e} \approx n_{0i} \approx 4.2 \times 10^{10} \text{ cm}^{-3}$. The remaining ground state atoms have no effect on the subsequent plasma dynamics, due to the short time scale of the experiment and the small neutral-ion collision cross-sections.

As a result of the much lighter mass of the electrons (compared to the heavy Sr ions), most of the excess energy from the photoionizing beam is acquired by the electrons, while the ions' kinetic energy remains similar to that of the neutral atoms in the MOT [41]. By tuning the wavelength of the pulsed dye laser, we vary the initial electron kinetic energies typically between 1 and 1000 K. The ion kinetic energy remains on the order of

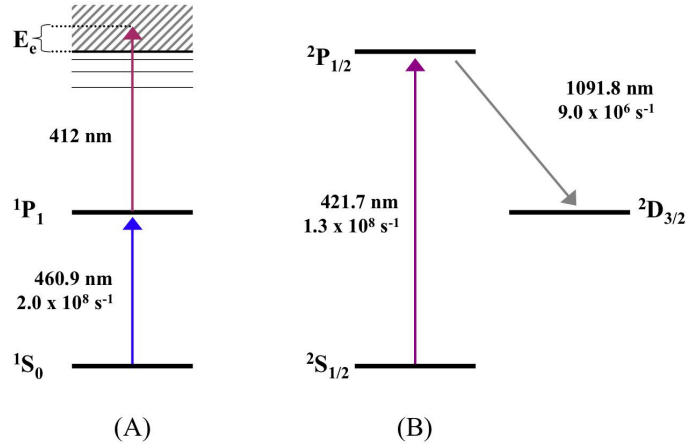


FIGURE 2. Relevant atomic and ionic energy levels of strontium, with corresponding decay rates. (A) Neutral atoms are laser-cooled and trapped in a MOT operating on the $^1S_0 - ^1P_1$ transition at 460.9 nm [45]. Atoms are excited to the 1P_1 level by a pulse-amplified laser and ionized by pulsed dye laser at ~ 412 nm. (B) Imaging of the ions is done on the $^2S_{1/2} - ^2P_{1/2}$ transition at 421.7 nm. $^2P_{1/2}$ ions decay to the $^2D_{3/2}$ state 7% of the time, after which they cease to interact with the probe beam. The intensity and duration of the 422 nm light is sufficiently low to avoid optical pumping to the metastable $^2D_{3/2}$ state.

millikelvin, close to the kinetic energy of neutral atoms in the MOT. However, disorder-induced heating [24, 29, 30] raises the temperature of the cold ions to approximately 1 K on the timescale of the inverse ion plasma oscillation frequency (~ 500 ns).

OPTICAL MODIFICATION OF VELOCITY DISTRIBUTIONS

The internal structure of the strontium ions relevant to our experiment can be represented by the simplified four level scheme depicted in Figure 3. Both the ground state ($5^2S_{1/2}$) and the excited state ($5^2P_{1/2}$) are doubly degenerate, where the total angular momentum projection can take on the values $m_j = +1/2$ and $m_j = -1/2$. The two ground states of the $5^2S_{1/2}$ level will be denoted by 1 ($m_j = -1/2$) and 3 ($m_j = +1/2$), and the two excited states of the $5^2P_{1/2}$ level will be denoted by 2 ($m_j = +1/2$) and 4 ($m_j = -1/2$).

The transitions between level 1 and 2 and between level 3 and 4 are driven by lasers with circularly polarized light, σ_+ and σ_- respectively, with frequencies ω_{ij} and Rabi frequencies

$$\Omega_{ij} = \frac{d_{ij}E_0}{\hbar}, \quad (1)$$

where E_0 is the field amplitude of the laser. The corresponding frequency detuning for each transition is $\Delta_{ij} = \omega_{ij} - \omega$, where $\hbar\omega = \Delta E$ is the energy difference between ground and excited state.

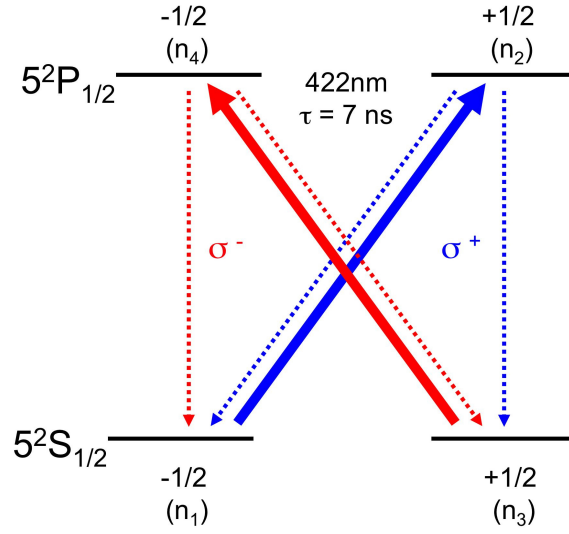


FIGURE 3. Simplified energy level schematic for the Sr^+ , where dashed lines indicate decay paths while solid lines indicate excitation paths. The $m_j = -1/2$ ($m_j = +1/2$) spin ground level is coupled to the higher energy $m_j = +1/2$ ($m_j = -1/2$) via σ^+ (σ^-) circularly polarized laser beam, from where it can decay back to either the $m_j = -1/2$ or $m_j = +1/2$. n_i labels the population of a particular spin state.

Ions in the excited states (2 and 4) decay to the ground states (1 and 3) with decay rates

$$\Gamma_{ij} = \frac{8\pi^2 d_{ij}^2}{3\epsilon_0 \hbar \lambda^3} \quad (2)$$

where d_{ij} is the dipol matrix element of the optical transition between level i and j , λ is the wavelength of the transition between ground and excited state, ϵ_0 is the electric constant and \hbar is the reduced Planck constant. For the total decay rate of levels 2 and 4 we have $\Gamma = \Gamma_{12} + \Gamma_{23} = \Gamma_{14} + \Gamma_{34}$, respectively.

Employing the rotating wave approximation one obtains the following optical Bloch equations for the density matrix of the four-level system

$$\dot{\rho}_{11} = i \frac{\Omega_{12}}{2} (\rho_{21} - \rho_{12}) + \Gamma_{12} \rho_{22} + \Gamma_{14} \rho_{44} \quad (3a)$$

$$\dot{\rho}_{22} = -i \frac{\Omega_{12}}{2} (\rho_{21} - \rho_{12}) - \Gamma \rho_{22} \quad (3b)$$

$$\dot{\rho}_{33} = i \frac{\Omega_{34}}{2} (\rho_{43} - \rho_{34}) + \Gamma_{23} \rho_{22} + \Gamma_{34} \rho_{44} \quad (3c)$$

$$\dot{\rho}_{44} = -i \frac{\Omega_{34}}{2} (\rho_{43} - \rho_{34}) - \Gamma \rho_{44} \quad (3d)$$

$$\dot{\rho}_{12} = -i \frac{\Omega_{12}}{2} (\rho_{11} - \rho_{22}) - \left(\frac{\Gamma}{2} + i \Delta_{12}\right) \rho_{12} \quad (3e)$$

$$\dot{\rho}_{13} = i \frac{\Omega_{12}}{2} \rho_{23} - i \frac{\Omega_{34}}{2} \rho_{14} \quad (3f)$$

$$\dot{\rho}_{14} = i \frac{\Omega_{12}}{2} \rho_{24} - i \frac{\Omega_{34}}{2} \rho_{13} - \left(\frac{\Gamma}{2} + i \Delta_{34}\right) \rho_{14} \quad (3g)$$

$$\dot{\rho}_{23} = i \frac{\Omega_{12}}{2} \rho_{13} - i \frac{\Omega_{34}}{2} \rho_{24} - \left(\frac{\Gamma}{2} - i \Delta_{12}\right) \rho_{23} \quad (3h)$$

$$\dot{\rho}_{24} = i \frac{\Omega_{12}}{2} \rho_{14} - i \frac{\Omega_{34}}{2} \rho_{23} - (\Gamma - i (\Delta_{12} - \Delta_{34})) \rho_{24} \quad (3i)$$

$$\dot{\rho}_{34} = -i \frac{\Omega_{34}}{2} (\rho_{33} - \rho_{44}) - \left(\frac{\Gamma}{2} + i \Delta_{34}\right) \rho_{34}. \quad (3j)$$

The diagonal elements ρ_{ii} are the populations of the four levels $i = 1, 2, 3, 4$ and ρ_{ij} , $i \neq j$ represent the coherences of the corresponding transitions.

At long times $t > \Gamma^{-1}$ one can adiabatically eliminate the coherences, i.e. set $\dot{\rho}_{ij} = 0$ for $i \neq j$, to rewrite Equations (3) in terms of a simple set of rate equations

$$\dot{f}_1(v) = +R_{12}(v)[f_2(v) - f_1(v)] + \Gamma_{12}f_2(v) + \Gamma_{14}f_4(v), \quad (4a)$$

$$\dot{f}_2(v) = -R_{12}(v)[f_2(v) - f_1(v)] - (\Gamma_{12} + \Gamma_{23})f_2(v), \quad (4b)$$

$$\dot{f}_3(v) = +R_{34}(v)[f_4(v) - f_3(v)] + \Gamma_{23}f_2(v) + \Gamma_{34}f_4(v), \quad (4c)$$

$$\dot{f}_4(v) = -R_{34}(v)[f_4(v) - f_3(v)] - (\Gamma_{14} + \Gamma_{34})f_4(v), \quad (4d)$$

for the velocity distributions $f_i = \rho_{ii}$ of ions in a given spin state i . The resulting pumping rates have a simple Lorentzian shape,

$$R_{ij}(v) = \frac{\Omega_{ij}^2/\Gamma}{1 + [2\Delta_{ij}/\Gamma]^2}. \quad (5)$$

As in the experiment two counterpropagating laser beams with same detuning Δ_{pump} and wavenumber $k = 2\pi/\lambda$ are used, the Doppler shift of an ion moving with velocity v in the directions of the lasers beams is accounted for by replacing $\Delta_{12} = \Delta_{\text{pump}} + kv$ and $\Delta_{34} = \Delta_{\text{pump}} - kv$ in Equations (3) and (5).

The simplified treatment of the rate equations (4) shows that the laser pumping transfers spin population between level 1 and 3 in the domain around the resonant

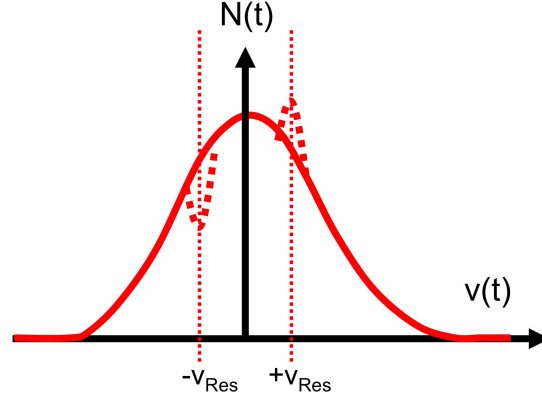


FIGURE 4. Cartoon of the expected velocity distribution for the $5^2S_{1/2}$ ($m_j = +1/2$), n_3 , with both counterpropagating pump lasers turned on (σ^- and σ^+). The solid line indicates the unperturbed distribution, while the dashed line indicate changes induced by optical pumping. A depletion of ion population is created as ions that meet the resonance condition $v_{Res} = \Delta_{pump}/k$ with the σ^- laser while an enhancement in ion population appears as ions from ($m_j = -1/2$) $5^2S_{1/2}$ (n_1) level are optically pumped by the σ^+ laser.

velocities $v_{res} = \pm \Delta_{pump}/k$, creating thereby an asymmetric velocity distribution as sketched in Figure 4.

Our experimental scheme to perform the described optical pumping and the resulting velocity distributions is shown in Figure 5. The two circularly polarized pump beams, with the same frequency yet opposite polarization and direction, interact with the plasma for a time of ~ 100 ns. For the strontium ion, the $S_{1/2} - P_{1/2}$ transition has a wavelength $\lambda = 421.7$ nm, and a total decay rate $\Gamma/(2\pi) = 21$ MHz. The σ^+ beam has an intensity of $I_{\sigma,+} = 334$ mW/cm² with beam waist of 1.18 mm, resulting in $\Omega_{12}/(2\pi) = 36.6$ MHz. On the other hand, the σ^- pumping beam has an intensity of $I_{\sigma,-} = 315$ mW/cm² with beam waist of 1.12 mm, resulting in $\Omega_{34}/(2\pi) = 35.0$ MHz. Furthermore, $\Delta_{pump}/(2\pi) = -20$ MHz. For these parameters the resonant velocity $|v_{res}| = 8.4$ m/s is well within the thermal velocity $\sqrt{k_B T/m} = 15$ m/s allowing for an efficient modification of the velocity distribution.

MEASUREMENT OF PERTURBED VELOCITY SPECTRA

At an adjustable time after optical pumping, a third, less intense σ^- circularly polarized probe beam, near resonant to the transition between level 3 and 4, propagates through the plasma (see Figure. 5). This probe beam has an intensity $I_{probe} = 73$ mW/cm² with beam waists of $w_z = 0.625$ mm and $w_x = 4.68$ mm. Laser-induced fluorescence in a perpendicular direction is then captured by a camera. The signal is spatially-resolved, so we can analyze the signal from different regions near the center of the plasma that have little variation in density and average plasma expansion velocity. By scanning the frequency detuning Δ of the probe beam, we obtain a spectrum $S(\Delta)$ that contains information on the ion velocity distribution. The measured fluorescence spectrum is

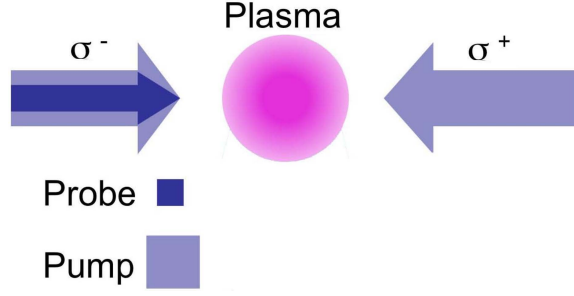


FIGURE 5. Experimental setup for optical modification of the ion velocity distribution in an UCP. The plasma cloud is illuminated by both the pump and probe beams originating from a 422 nm laser, that is near resonant with the $S_{1/2} - P_{1/2}$ transition of Sr^+ . The pump beams have the same laser frequency yet opposite circular polarization and travel in opposite directions. The probe beam has σ^- circular polarization and can be scanned to obtain a fluorescence spectrum by capturing the probe-beam induced fluorescence light with a CCD-intensified camera perpendicular to the beam direction.

proportional to the velocity-dependent population of the ground state f_3 convolved with the Lorentzian excitation profile of the probe beam, i.e.

$$S(\Delta) \propto \int f_3(v) L(v, \Delta) dv, \quad (6)$$

$$L(v, \Delta) \propto \frac{1}{1 + s_{0,\text{probe}} + [2(\Delta - kv)/\Gamma_{\text{tot}}]^2}, \quad (7)$$

where, $\Gamma_{\text{tot}} = \Gamma + \Gamma_{\text{inst}}$ is the total linewidth, $\Gamma_{\text{inst}}/(2\pi) = 7 \text{ MHz}$ is the instrumental laser linewidth and $s_{0,\text{probe}} = I_{\text{probe}}/I_{\text{sat}}$. The saturation intensity for the $S_{1/2} - P_{1/2}$ transition with circular polarized light is $I_{\text{sat}} = 57 \text{ mW/cm}^2$.

Figure 6 shows ion spectra measured after 100 ns of optical pumping and, for comparison, ion spectra without optical pumping, for a plasma with ion temperature $T_i = 2.3 \text{ K}$, density $n_0 = 3.1 \times 10^{15} \text{ m}^{-3}$ and coupling parameter $\Gamma_i = 1.7$. The spectra are scaled by the maximum of each curve. We record separately the spectra for three regions around plasma center (labeled Region -1, 0, 1). Given the higher mean velocity in the outer regions due to plasma expansion [47], their corresponding spectra are shifted from zero (Regions ± 1). Notice the depletion in ion population for $\Delta/(2\pi) \approx -20 \text{ MHz}$ and enhancement in ion population for $\Delta/(2\pi) \approx 20 \text{ MHz}$ in region 0, as discussed above. The features here are less sharp, compared to the schematic distribution of Figure 4 due to power broadening from the pump beams [44] and the convolution of the velocity distribution and Lorentzian excitation profile (Equation 6). As the probe and pump pulses originate from the same laser source, the probe pulse has a limited frequency scanning range, resulting in the narrow range from about -50 to 50 MHz (see Figure 6), which complicates the analysis of the experimental data.

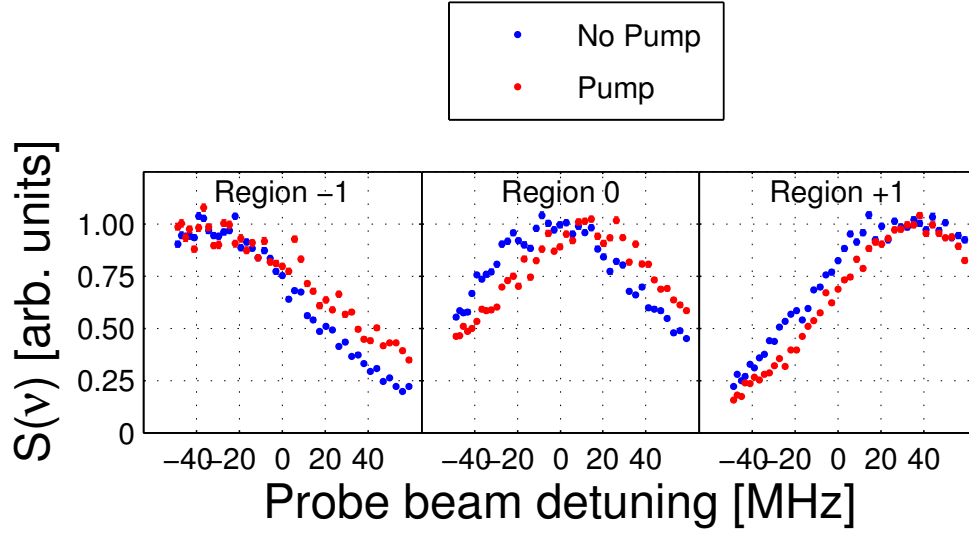


FIGURE 6. Ion spectra for 3 regions around plasma center with (red dots) and without (blue dots) pump beams for $T_i = 2.3$ K, $n_0 = 3.1 \times 10^{15} \text{ m}^{-3}$ and $\Gamma_i = 1.7$. The spectra were measured $0.13 \mu\text{s}$ after optical pumping and are normalized by scaling to the maximum of each curve. To achieve low Γ_i , we allow the plasma cloud to expand significantly before applying the pump beams. As a consequence regions other than plasma center have significant expansion velocity and display significant shift in their spectra. Notice the depletion in ion population for $\Delta/(2\pi) \approx -20$ MHz and enhancement for $\Delta/(2\pi) \approx +20$ MHz.

EXTRACTING THE VELOCITY DISTRIBUTION

As described in the previous section, the reconstruction of the underlying velocity distribution from the recorded ion spectra is complicated due to experimental limitations on the accessible frequency range. This leads to a loss of information contained in the wings of the spectrum. To determine possible errors of the reconstruction process, we performed numerical simulations of the experiment, which provide spectral information over the full frequency range, and can thus be used for accurate comparisons of the real and extracted velocity distribution, as obtained from a finite frequency range of the simulated spectra.

The ion dynamics including the collisional redistribution of velocities can be accurately captured by classical molecular dynamics (MD) simulations. The ions are represented by an one-component plasma of N particles in a cubic simulation cell with periodic boundary conditions. The mutual interactions of the ions are effectively treated by the fast multipole method [48, 49, 50], which permits force calculations for large particle numbers with a numerical effort that scales only linearly with the number of ions.

The optical pumping process is described by solving the optical Bloch equations (3) along each ion trajectory. The internal state dynamics is included by assigning the four-level density matrix $\rho^{(q)}$ to each of the $q = 1, \dots, N$ ions. Initially the two ground states are equally populated, i. e. $\rho_{11}^{(q)} = \rho_{33}^{(q)} = 0.5$, and $\rho_{ij}^{(q)} = 0$ for all remaining matrix elements. For the duration of the pump pulse we solve the optical Bloch equations (3)

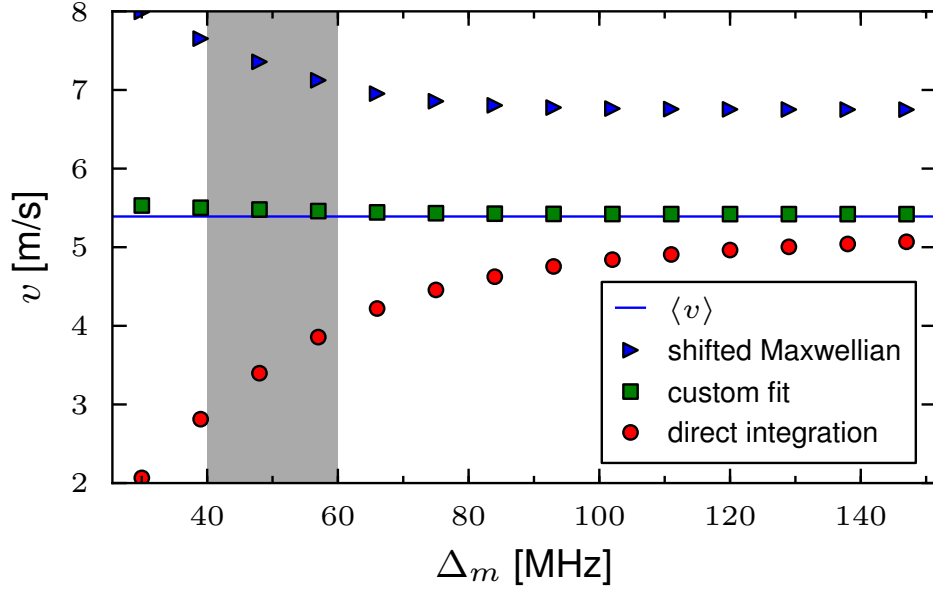


FIGURE 7. Comparison of the true average velocity $\langle v \rangle$ (blue line) to the average velocity as obtained from different extraction procedures using the frequency range $(-\Delta_m, \Delta_m)$ of the simulated spectrum. Direct integration of the spectrum using Equation (9) and the shifted Maxwellian center velocity v_c show significant deviations within the experimentally available frequency range $\Delta_m/(2\pi) \approx 50$ MHz (shaded grey), whereas excellent agreement for the average velocity is obtained from the fit formula (13).

numerically for each ion individually, taking into account the time-dependent laser detuning due to the changing ion velocity obtained from the MD simulation. From the simulated velocity distributions $f_i(v, t)$, we obtain the fluorescence spectra by convolution with the Lorentzian emission profile (7) according to Equation (6).

With the simulated spectra at hand, we can now proceed to analyze possible schemes to extract the velocity distribution from the finite frequency range of the experimental fluorescence spectra. To assess the quality of the different methods, we use the average velocity $\langle v \rangle$ as a figure of merit.

Given the entire excitation spectrum, $S(\Delta)$, the average velocity is related to the average frequency shift through the wavenumber of the probe beam, k , according to

$$\langle \Delta \rangle = \frac{\int_{-\infty}^{\infty} \Delta S(\Delta) d\Delta}{\int_{-\infty}^{\infty} S(\Delta) d\Delta} = k \langle v \rangle. \quad (8)$$

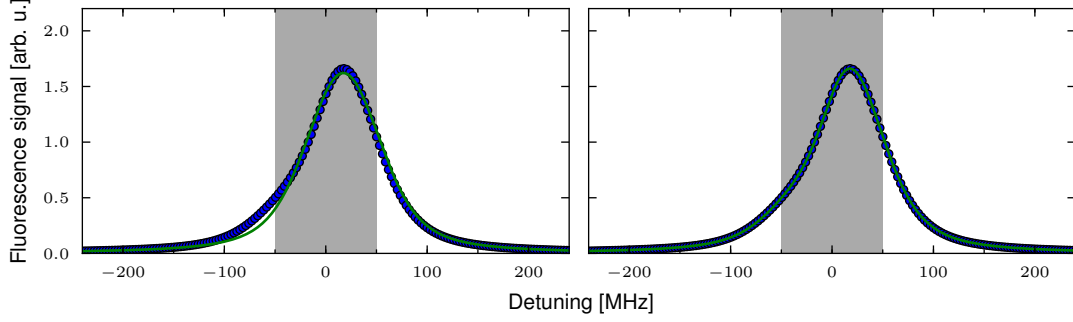


FIGURE 8. Fit (green line) of a convoluted Maxwellian (left) and of equation (13) (right) to the simulated spectrum (symbols) corresponding to $T = 2.8$ K, $\rho = 13 \times 10^9 \text{ cm}^{-3}$, $\Gamma = 1.4$. In each case the fit is only applied in the interval $(-50, 50)$ MHz (shaded gray area).

From a limited portion of the spectrum, $-\Delta_m < \Delta < \Delta_m$, if one makes a Taylor expansion of the integrand in Equation (6) around $v = 0$, the relation can be written as

$$\langle \Delta \rangle = \frac{\int_{-\Delta_m}^{\Delta_m} \Delta S(\Delta) d\Delta}{\int_{-\Delta_m}^{\Delta_m} S(\Delta) d\Delta} \approx \kappa(\Delta_m) \langle v \rangle \quad (9)$$

The frequency-interval dependent proportionality constant is given by

$$\kappa(\Delta_m) = k \left(1 - \frac{2 \Delta_m / \Gamma}{\left(1 + (2 \Delta_m / \Gamma)^2 \right) \arctan(2 \Delta_m / \Gamma)} \right) \quad (10)$$

and recovers Equation (8) in the limit $\Delta_m \rightarrow \infty$. As shown in Figure 7 this procedure yields the correct average velocity for large Δ_m , but significantly underestimates the correct value of $\langle v \rangle$ for the experimentally measurable region ($\Delta_m \sim 50$ MHz).

An alternative method, which works well for our data, is to assume a specific form for the velocity distribution and vary the parameters of the distribution to fit the resulting excitation spectrum to the experimental measurements. For an appropriate choice of the functional form of the velocity distribution, this allows accurate approximation of the full velocity distribution based on finite spectral information.

A simple ansatz is to assume that the velocity distribution after pumping still retains its Maxwellian shape but is only shifted by an amount v_c from zero. Figure 8a shows the fit of a convoluted, shifted Maxwellian to the simulated spectrum using only the experimentally available frequency range (shaded gray area). We find good agreement between fit and data in the central, observable part of the spectrum, but slight deviations at larger frequencies beyond the experimentally available data. These small discrepancies can cause considerable deviations of the average velocity as shown Figure 7.

The situation can be improved by using a fit formula that captures the effects of optical pumping and the collisional redistribution of velocities more accurately. In order

to construct such an expression we start from the rate equations (4) and adiabatically eliminate the dynamics of the excited state populations f_2 and f_4 . Collisional effects are accounted for within the relaxation time approximation [51] which gives

$$\dot{f}_1(v) = R_{\leftarrow}(v) f_3(v) - R_{\rightarrow}(v) f_1(v) - \gamma \left[f_1(v) - \frac{1}{2} f_M(v) \right], \quad (11a)$$

$$\dot{f}_3(v) = R_{\rightarrow}(v) f_1(v) - R_{\leftarrow}(v) f_3(v) - \gamma \left[f_3(v) - \frac{1}{2} f_M(v) \right], \quad (11b)$$

where γ is an effective relaxation rate and $f_M(v) = f_1(v) + f_3(v)$ denotes the Maxwellian velocity distribution at a given temperature. Moreover, the transition rates R_{\rightarrow} and R_{\leftarrow} for a transition from state 1 to state 3 and vice versa are obtained from the rate equations (4) according to

$$R_{\rightarrow}(v) = \frac{R_{12}(v) \Gamma_{23}}{\Gamma + R_{12}(v)}, \quad (12a)$$

$$R_{\leftarrow}(v) = \frac{R_{34}(v) \Gamma_{14}}{\Gamma + R_{34}(v)}. \quad (12b)$$

From the steady state ($\dot{f}_1(v) = \dot{f}_3(v) = 0$) of these equations we obtain the following simple fit formula

$$f_3(v) = f_M(v) \frac{\frac{a_1}{1+b_1(v_{\text{res}}+v)^2} + \frac{1}{2}}{\frac{a_1}{1+b_1(v_{\text{res}}-v)^2} + \frac{a_2}{1+b_2(v_{\text{res}}+v)^2} + 1}. \quad (13)$$

For steady state conditions, the parameters a_1, a_2, b_1 and b_2 can be expressed in terms of the parameters of Equations (11) and (12). In most cases, however, the system does not reach the steady state for our experimental parameters and optical pumping times. Nevertheless, one can apply Equation (13) to fit the measured spectra using a_1, a_2, b_1, b_2 as free parameters. As we will show below, this ansatz indeed provides an excellent description of the actual velocity distributions. The parameters a_1, a_2 quantify the importance of optical pumping relative to collisional redistribution and the parameters b_1, b_2 control the widths of the asymmetric features of the velocity distribution. In the limit $a_1, a_2 \gg 1$, Equation (13) yields the correct steady state for very strong pumping and weak collisions. On the other hand, for $a_1, a_2 = 0$ it recovers the equilibrium Maxwell distribution, as expected in the absence of optical pumping.

As shown in Figure 8b, the frequency spectrum obtained from convolving Equation (13) according to Equation (7) yields a much improved fit as compared to the shifted Maxwellian, shown in Figure 8a. Moreover it accurately describes the wings of the spectrum, even though the fitting has been determined from the finite frequency range $-50 \text{ MHz} < \Delta < 50 \text{ MHz}$. Consequently, the extracted average velocity, shown in Figure 7, is in excellent agreement with the real value of $\langle v \rangle$ even for a very limited range of frequencies available for fitting the fluorescence spectrum. Moreover, the procedure described above can also be used to construct reliable fitting functions for more complex optical pumping schemes that may be applied in future experiments.

SUMMARY

In this work we have presented new techniques to perturb, probe, and model ion velocity distributions in ultracold neutral plasmas. We anticipate that the described approach will serve as a valuable tool for direct experimental measurements of non-equilibrium plasma dynamics in the regime of strong coupling.

ACKNOWLEDGMENTS

This work was supported by the Department of Energy and National Science Foundation (PHY-0714603).

REFERENCES

1. F. Anderegg, C. F. Driscoll, D. H. E. Dubin, and T. M. O'Neil. Wave-particle interactions in electron acoustic waves in pure ion plasmas. *Phys. Rev. Lett.*, 102:095001, 2009.
2. J. J. Curry, F. Skiff, M. Sarfaty, and T. N. Good. Measurement of fokker-planck diffusion with laser-induced fluorescence. *Phys. Rev. Lett.*, 74:1767, 1995.
3. M. J. Jensen, T. Hasegawa, J. J. Bollinger, and D. H. E. Dubin. Rapid heating of a strongly coupled plasma near the solid-liquid phase transition. *Phys. Rev. Lett.*, 94:025001, 2005.
4. W. Happer. Optical pumping. *Rev. Mod. Phys.*, 44:169, 1972.
5. J. Amorim, G. Baravian, and J. Jolly. Laser-induced resonance fluorescence as a diagnostic technique in non-thermal equilibrium plasmas. *J. Phys D.*, 33:R51, 2000.
6. S. Mondal, Amit D. Lad, Saima Ahmed, V. Narayanan, J. Pasley, P. P. Rajeev, A. P. L. Robinson, and G. Ravindra Kumar. Doppler spectrometry for ultrafast temporal mapping of density dynamics in laser-induced plasmas. *Phys. Rev. Lett.*, 105:105002, 2010.
7. T. C. Killian, S. Kulin, S. D. Bergeson, L. A. Orozco, C. Orzel, and S. L. Rolston. Creation of an ultracold neutral plasma. *Phys. Rev. Lett.*, 83(23):4776–4779, Dec 1999.
8. J. P. Morrison, C. J. Rennick, J. S. Keller, and E. R. Grant. Evolution from a molecular rydberg gas to an ultracold plasma in a seeded supersonic expansion of no. *Phys. Rev. Lett.*, 101(20):205005, Nov 2008.
9. S. D. Bergeson and R. L. Spencer. *Phys. Rev. E*, 67:026414, 2003.
10. R. S. Fletcher, X. L. Zhang, and S. L. Rolston. *Phys. Rev. Lett.*, 96:105003, 2006.
11. J. T. Mendonca, J. Loureiro, and H. Tercas. *Journal of Plasma Physics*, 75(06):713, 2009.
12. J. Castro, P. McQuillen, and T. C. Killian. *Phys. Rev. Lett.*, 105:065004, 2010.
13. A. Lyubonko, T. Pohl, and J.M. Rost. *arXiv:1011.5937*, 2010.
14. J. T. Mendonca and P. K. Shukla. *Phys. Plasmas*, 18:042101, 2011.
15. P. K. Shukla. *Phys. Lett. A*, 374:3656, 2011.
16. S. Kulin, T. C. Killian, S. D. Bergeson, and S. L. Rolston. *Phys. Rev. Lett.*, 85:318, 2000.
17. F. Robicheaux and J. D. Hanson. *Phys. Rev. Lett.*, 88:055002, 2002.
18. F. Robicheaux and J. D. Hanson. *Phys. Plasmas*, 10:2217, 2003.
19. T. Pohl, T. Pattard, and J. M. Rost. *Phys. Rev. A*, 68:010703, 2003.
20. T. Pohl, T. Pattard, and J. M. Rost. *Phys. Rev. A*, 70:033416, 2004.
21. S. Laha, P. Gupta, C. E. Simien, H. Gao, J. Castro, T. Pohl, and T. C. Killian. *Phys. Rev. Lett.*, 99:155001, 2007.
22. K. A. Twedt and S. L. Rolston. *Phys. Plasmas*, 17:082101, 2010.
23. J. P. Morrison, C. J. Rennick, and E. R. Grant. Very slow expansion of an ultracold plasma formed in a seeded supersonic molecular beam of no. *Phys. Rev. A*, 79(6):062706, Jun 2009.
24. M. S. Murillo. *Phys. Rev. Lett.*, 87:115003, 2001.
25. S. Mazevet, L. A. Collins, and J. D. Kress. *Phys. Rev. Lett.*, 88:055001, 2002.
26. S. G. Kuzmin and T. M. O'Neil. *Phys. Rev. Lett.*, 88:065003, 2002.

27. T. Pohl, T. Pattard, and J. M. Rost. Coulomb crystallization in expanding laser-cooled neutral plasmas. *Phys. Rev. Lett.*, 92:155003, 2004.
28. C. E. Simien, Y. C. Chen, P. Gupta, S. Laha, Y. N. Martinez, P. G. Mickelson, S. B. Nagel, and T. C. Killian. *Phys. Rev. Lett.*, 92:143001, 2004.
29. Y. C. Chen, C. E. Simien, S. Laha, P. Gupta, Y. N. Martinez, P. G. Mickelson, S. B. Nagel, and T. C. Killian. *Phys. Rev. Lett.*, 93:265003, 2004.
30. T. Pohl, T. Pattard, and J. M. Rost. Relaxation to nonequilibrium in expanding ultracold neutral plasmas. *Phys. Rev. Lett.*, 94:205003, 2005.
31. E. A. Cummings, J. E. Daily, D. S. Durfee, and S. D. Bergeson. *Phys. Rev. Lett.*, 95:235001, 2005.
32. P. K. Shukla and K. Avinash. *Phys. Rev. Lett.*, 107:135002, 2011.
33. T. C. Killian, M. J. Lim, S. Kulin, R. Dumke, S. D. Bergeson, and S. L. Rolston. Formation of rydberg atoms in an expanding ultracold neutral plasma. *Phys. Rev. Lett.*, 86:3759, 2001.
34. P. Gupta, S. Laha, C. E. Simien, H. Gao, J. Castro, T. C. Killian, and T. Pohl. *Phys. Rev. Lett.*, 99:075005, 2007.
35. R. S. Fletcher, X. L. Zhang, and S. L. Rolston. Using three-body recombination to extract electron temperatures of ultracold plasmas. *Phys. Rev. Lett.*, 99(14):145001, Oct 2007.
36. T. Pohl, D. Vrinceanu, and H. R. Sadeghpour. Rydberg atom formation in ultracold plasmas: Small energy transfer with large consequences. *Phys. Rev. Lett.*, 100(22):223201, Jun 2008.
37. S. D. Bergeson and F. Robicheaux. *Phys. Rev. Lett.*, 101:073202, 2008.
38. G. Bannasch and T. Pohl. Rydberg atom formation in strongly correlated ultracold plasmas. *ArXiv*, 1109.6456:2011, *Phys. Rev. A*, to be published.
39. X. L. Zhang, R. S. Fletcher, and S. L. Rolston. *Phys. Rev. Lett.*, 101:195002, 2008.
40. M. Rosenberg and P. K. Shukla. *Physica Scr.*, 83:015503, 2011.
41. T. C. Killian, T. Pattard, T. Pohl, and J. M. Rost. Ultracold neutral plasmas. *Phys. Rep.*, 449(4-5):77 – 130, 2007.
42. T. C. Killian. *Science*, 316:705, 2007.
43. T. C. Killian and S. L. Rolston. *Phys. Today*, 63:46, 2010.
44. H. J. Metcalf and P. van der Straten. *Laser Cooling and Trapping*. Springer-Verlag, New York, 1999.
45. S. B. Nagel, C. E. Simien, S. Laha, P. Gupta, V. S. Ashoka, and T. C. Killian. Magnetic trapping of metastable 3P_2 atomic strontium. *Phys. Rev. A*, 67:011401, Jan 2003.
46. S. B. Nagel, P. G. Mickelson, A. D. Saenz, Y. N. Martinez, Y. C. Chen, T. C. Killian, P. Pellegrini, and R. Côté. Photoassociative spectroscopy at long range in ultracold strontium. *Phys. Rev. Lett.*, 94:083004, Mar 2005.
47. J. Castro, H. Gao, and T. C. Killian. Using sheet fluorescence to probe ion dynamics in an ultracold neutral plasma. *Plasma Phys. Control. Fusion*, 50:124011, 2008.
48. L. Greengard and V. Rokhlin. A fast algorithm for particle simulations. *J. Comput. Phys.*, 73(2):325 – 348, 1987.
49. Holger Dachsels. *J. Chem. Phys.*, 132(11):119901, 2010.
50. H. Dachsels and I. Kabadshow. www.fz-juelich.de/jsc/fmm.
51. M. Bonitz and D. Kremp. Kinetic energy relaxation and correlation time of nonequilibrium many-particle systems. *Physics Letters A*, 212(1-2):83, 1996.